

RADIO INTERFACE DESIGN FOR INKJET-PRINTED BIOSENSOR APPLICATIONS

Janne Jalo, Hannu Sillanpää* , and Riku Mäkinen

Department of Electronics and Communications Engineering, Tampere University of Technology, P. O. Box 692, Tampere FI-33101, Finland

Abstract—Biomedical wireless sensors require thin, lightweight, and flexible single-layer structures operating in immediate proximity of human body. This poses a challenge for RF and antenna design required for wireless operation. In this work, the radio interface design for a 2.4 GHz wireless sensor including a discrete filter balun circuit and an antenna operating at 0.3 mm distance from the body is presented. Thin, lightweight single-layer structure is realized using printed electronics manufacturing technology. The RF and antenna designs are validated by measurements, and a sensor with a fully functional radio interface is implemented and verified. At 0.3 mm from the body, 2.4 dB insertion loss and -10 dBi realized gain at 2.4 GHz were achieved for a discrete filter balun and antenna, respectively. The received power level on a Bluetooth low energy (BLE) channel was above -80 dBm at 1 m distance from the body, indicating capability for short-range off-body communications. The paper also provides guidelines for printed electronics RF and antenna design for on-body operation.

1. INTRODUCTION

Thin electronics structures enable plaster-like sensors that can be attached directly to the skin and used to measure various physiological signals [1]. Printed electronics technology including digital inkjet printing [2] can be used to realize thin, lightweight, and flexible single-layer structures making it well suited for thin and flexible body-worn wireless sensor applications. Inkjet technology has been successfully demonstrated for system integration [3], radio frequency (RF) circuits [4], and antenna applications [5, 6].

Received 13 June 2013, Accepted 15 August 2013, Scheduled 10 September 2013

* Corresponding author: Hannu Sillanpää (hannu.sillanpaa@tut.fi).

The deteriorating effect of the human body on antenna characteristics is well known [7–14]. However, the body effects on other RF structures and circuits have received little attention. The research [15] has shown, that at distances less than 0.5 mm from the body can have effect on characteristic impedances and losses of RF interconnections. According to another research [16], the operation of simple discrete RF circuits can be significantly tuned in close proximity of human body. Previous research indicates that the body effects need to be considered for both RF and antenna design. This is of particular interest for biosensors operating in immediate proximity of the body.

In this work, the design of an inkjet-printed wireless sensor at 2.4 GHz designed to operate at 0.3 mm distance from the body is presented. The radio interface consists of a system-on-chip (SoC), a discrete filter balun circuit, and an antenna. The prototypes were inkjet-printed with Harima NPS-JL silver nanoparticle ink on a 50- μm polyethylene naphthalate (PEN) substrate. The operation of the filter balun was validated by using vector network analyzer (VNA) with a probe station whereas the antenna designs were validated with Satimo StarLab measurements using fresh beef to model human body. Finally, the on-body operation of a full radio interface of the sensor was validated by establishing a radio link and measuring the received power on a Bluetooth low-energy (BLE) channel.

The rest of the paper is organized as follows. The discrete filter balun design including modeling, design, and validation is described in Section 2. Finally, on-body antennas and a full radio interface for biosensor applications are presented in Section 3. Section 4 concludes the paper.

2. ON-BODY DISCRETE RF CIRCUIT DESIGN

The on-body discrete RF design is discussed in the context of a discrete filter balun circuit operating at 2.4 GHz. The design is carried out using AWR Microwave Office.

2.1. Design Methods

The materials used include silver nanoparticle ink, PEN substrate, 0.3 mm plaster used as spacer, and muscle tissue used as a simplified human body model. The electrical properties of the dielectric and conductor layers are listed in Table 1. The parameters for the conductor were obtained from the average dc sheet resistance $R_s = 40 \text{ m}\Omega/\square$ measured from 10 Greek cross [17] test structures. High-frequency analysis with multilayer characterization method [18–20]

Table 1. Electrical properties of the dielectric and conductor layers for EM simulations.

Dielectric layer	Thickness (μm)	ϵ_r	$\tan \delta$	σ_{cond} (S/m)
Conductor	1	—	—	$1.25 * 10^7$
Substrate	50	2.9	0.006	—
Plaster	300	1.4	0.02	—
Muscle tissue	5000	[15, 22]	[15, 22]	—

based on multilayer Thru-Reflect-Line (TRL) calibration [21] confirmed the validity of using the dc value at 2.4 GHz. The loss tangent and relative permittivity of human body are available at [22] from which they were defined for simulations as frequency dependent parameters [15]. For on-body operation, a 0.3 mm thick layer of plaster (polyacrylate, with $\epsilon_r = 1.4$ and $\tan \delta = 0.02$) was used between the body and sensor. Previous work indicates that manufacturer's component models based on measurements on FR4 board may be inaccurate when components are placed on thin polymer film substrate [16]. Therefore both library components and component values measured on PEN substrate with microwave probe station and ground-signal-ground (GSG) probes were considered for circuit design.

A filter balun circuit was designed to match the differential input impedance $Z = 6.7 - j107 \Omega$ of the RF SoC to 50Ω at the single-ended antenna port. The design was optimized for inkjet-printed interconnections on polymer substrate by tuning the component values. The layout for the electromagnetic (EM) modeling is shown in Fig. 1, with the location of passive components as well as differential (DIFF) and single-ended (SE) ports indicated in the layout. The schematic is omitted for brevity. The inductor L_1 introducing a 180° phase shift between the differential port is critical for the design. Capacitors C_4 through C_6 and inductor L_3 provide impedance matching and filtering. The operation voltage is connected at the node between L_2 and C_7 . The decoupling capacitor C_7 has no effect on RF operation and could be replaced with a short circuit with no effect on the results. The overall size of the layout is approximately $10 \text{ mm} \times 6 \text{ mm}$.

The components used for the filter balun were C1005 series capacitors from TDK and LQW15 series inductors from Murata. To investigate the design accuracy, the filter balun was modeled using both AWR library components and measured component models. The measured components included a short 0.5 mm transmission line at both ends of the component. Therefore, multilayer TRL calibration [21] standards were included in the print file to de-embed the test fixture

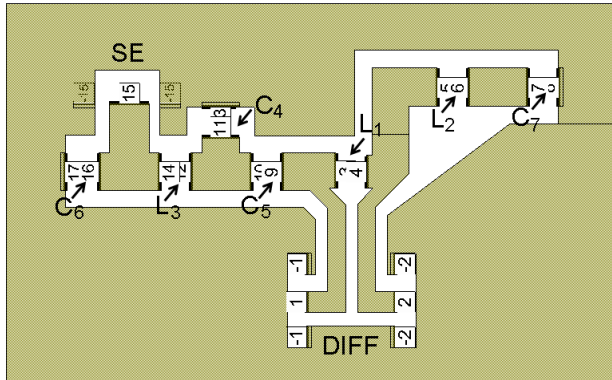


Figure 1. Layout of the filter balun. The nominal component values are (size 0402): $L_1 = L_3 = 4.7$ nH, $L_2 = 15$ nH, $C_4 = C_6 = 0.75$ pF, $C_5 = 1.8$ pF, and $C_7 = 2.2$ nF.

effects. Passivity was enforced on the calibrated components to remove possible amplification due to slight calibration and measurement inaccuracy. Note that slight amplification is sometimes observed also with the manufacturer's component library S parameter files.

2.2. Measurement Setup

Filter baluns were measured with a two-port HP8722D VNA and microwave probe station with $800\ \mu\text{m}$ GSG probes. Probe-tip Short-Open-Load-Thru (SOLT) calibration was performed with Cascade Microtech 106-682 impedance standard substrate (ISS). Filter baluns were measured two ports at a time with the additional port terminated to a $50\ \Omega$ resistor, requiring measurement of three prototypes to construct three-port S parameters [23].

The prototypes were first measured on Rohacell HF31 microwave foam ($\epsilon_r = 1.05$ and $\tan \delta < 0.0002$ at 3 GHz) to provide information on modeling accuracy without the plaster and body tissue. After this, filter baluns were placed on $300\ \mu\text{m}$ thick plaster which is then placed on $5\ \text{mm}$ thick layer of fresh beef emulating the properties of the human muscle. The measurement setup is shown in Fig. 2.

2.3. On-body Design and Validation

The results are analyzed using the mixed-mode S parameters [24]. Figs. 3 and 4 show the differential mode reflection S_{dd22} and single-ended mode reflection S_{ss11} and the single-ended to differential mode

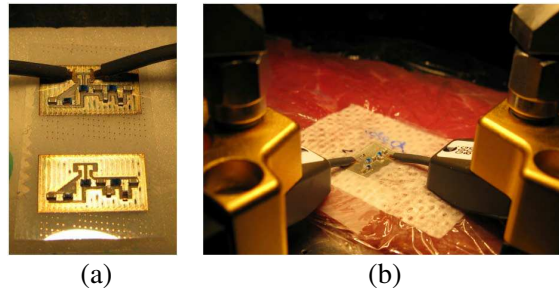


Figure 2. Filter baluns measured (a) on Rohacell HF31 microwave foam and (b) on beef.

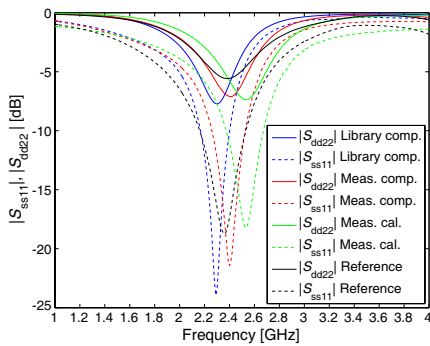


Figure 3. Measured reference and simulated S_{ss11} (single-ended port) and S_{dd22} (differential port) in air.

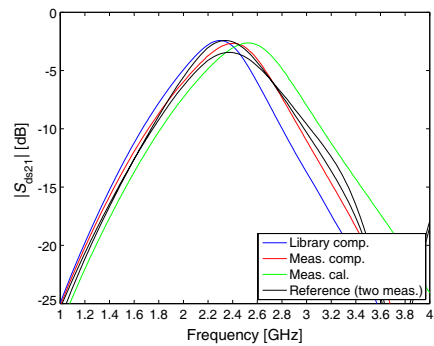


Figure 4. Measured reference and simulated S_{ds21} in air.

transmission S_{ds21} for the filter balun measured and simulated in air. Three types of component models are considered including manufacturer’s component libraries and measured component values both with and without multiline calibration to remove the effects of the test fixtures.

The library components show a shift in frequency toward dc since they are based on measurements on thick FR4 substrate and therefore, cause inaccuracies in simulations with thin flexible substrate without backing ground plane. Whereas with the measured calibrated components the operation frequency is shifted to a higher frequency because the circuit is sensitive to even small measurement errors. However, the differences between measurements and simulations are small in all the cases. Best agreement is obtained with measured

component values without calibration, that however contain additional 0.5 mm transmission lines at both ends. For the circuit in Fig. 1, the critical component is L_1 introducing a 180° phase shift at the differential port. A small change in the value of L_1 directly affects the center frequency of the filter balun. Also the length of the differential line between the input of the RF SoC and L_1 has a similar effect. Consequently, a slight shift in the reference plane in the component measurement or multiline TRL calibration of L_1 may introduce the change in operation frequency observed for the measured calibrated components. Despite this, all component models considered show relatively good agreement with the measured results and can be used for discrete RF design for inkjet technology.

Following [15], the presence of body was considered in simulations using the material parameters listed in Table 1. The effect of body is illustrated in Fig. 5, where the simulated differential to single-ended transmission S_{ds21} is shown at different distances from the body. The limiting cases are the circuit located in free space (with 300 μm plaster substrate) and in direct contact with the body. In other simulations, the thickness of the plaster between the body and the PEN substrate is varied. At 300 μm from the body, the results converge toward the free-space simulation. There is only a slight shift in operation frequency, indicating 0.3 mm to be a safe distance. This is in agreement with [15], where the body effect on high-frequency interconnections was found to be small already at 200 μm from the body.

Based on the above analysis, the filter balun was designed with a 300 μm thick plaster placed between the PEN substrate and muscle tissue. Fig. 6 shows the simulated and measured on-body S_{ds21} for the circuit. The three component models considered perform in a

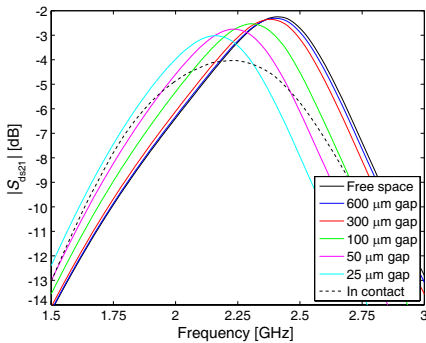


Figure 5. Simulated S_{ds21} as a function of distance to the body.

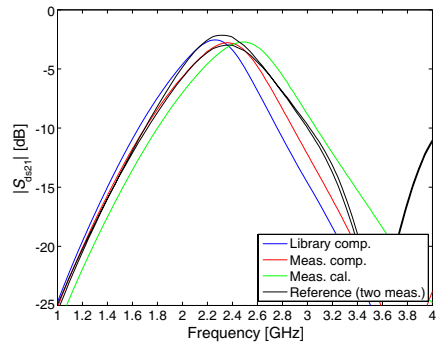


Figure 6. Measured reference and simulated S_{ds21} on body.

similar manner as without the body, indicating the modeling approach is valid also for on-body design. Finally, the body effect is shown in more detail in Fig. 7, where measured results for the LC filter balun and a commercial monolithic component are presented. As predicted by simulations, the 300 μm distance from the body slightly tunes the center frequency of the circuits when compared to the measurements performed on microwave foam. For both LC and monolithic balun circuits, the shift in frequency due to the body is approximately 50 MHz. The apparent 0.2 dB reduction in loss for the LC balun in the presence of the body is within the measurement uncertainty.

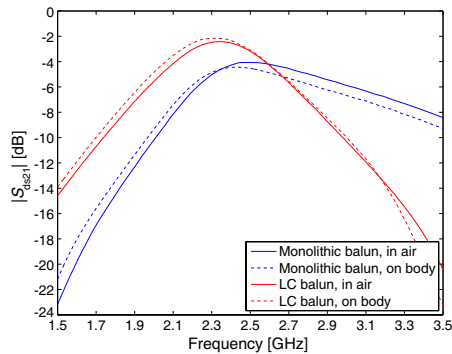


Figure 7. Measured results for LC filter balun and a commercial monolithic balun component from ST microelectronics.

3. PRINTED WIRELESS SENSOR APPLICATION

3.1. Sensor Layouts

Reference [10] compares the performance of electric and magnetic antennas close to the body. In immediate proximity at 0.3 mm and 0.6 mm from the body, magnetic antennas were found to perform the best. Both simulations and measurements indicated -11 dBi maximum realized gain (including mismatch loss) for an inkjet-printed magnetic half-wave slot antenna [10]. The half-wave slot presented in [10] was redesigned and integrated with the sensor electronics. The layouts are shown in Fig. 8.

3.2. On-body Antenna Performance

The sensor antennas with electronics were redesigned by simulations as described in [10]. Two versions with slightly different routing were considered. The antennas were optimized to operate at 0.3 mm



Figure 8. Sensor layouts for antenna measurements. The size of the sensors is $45\text{ mm} \times 22.5\text{ mm}$. (a) Sensor 1, (b) sensor 2.



Figure 9. (a) Sensor measurement setup and (b) measured sensor prototypes.

or 0.6 mm from the body. At these distances, the return loss (not shown) was above 10 dB at the 2.4 GHz band but increasing toward 3 GHz . The on-body operation was verified by measurements using the measurement setup and prototypes shown in Fig. 9. A $20\text{ cm} \times 20\text{ cm} \times 5\text{ cm}$ piece of fresh beef weighing approximately 2 kg was used to model the body. The antennas were measured at 0.3 mm (one plaster), 0.6 mm (two plasters), and 2 mm (Rohacell HF31) from the body. Measurements in direct contact and in free space were also carried out for completeness.

The key dimensions and measurement results of the different antennas on body at 2.44 GHz are summarized in Table 2 [10]. The measured maximum realized gain is shown in Fig. 10. The magnetic antenna without sensor electronics reported in [10] was re-measured and used as a reference to verify the properties of the sample of beef used in the measurements did not differ from that previously used. For the reference antenna, the realized gain at 2.4 GHz band is approximately -10 dBi at both 0.3 mm and 0.6 mm distance from the body. For both sensor prototypes, the gain is approximately -12 dBi

Table 2. Comparison of sensor antennas [10]. Key dimensions and measured properties at 2.44 GHz with antennas placed at 0.3 mm from the body.

Antenna	Key Dimension	Total area (mm ²)	Return Loss (dB)	Max Gain (dBi)	η_{tot} (dB)
Magnetic dipole	length 40 mm	50 × 31	11.3	-11.4	-18.0
Inverted F (large)	F length 36.7 mm	50 × 28.4	8.6	-16.6	-22.7
Inverted F (small)	F length 17 mm	40 × 19.6	12.5	-15.1	-20.7
Annular slot with T feed	slot 40.8 × 17.8 mm ²	45 × 22	3.7	-17.7	-24.0
Meander structure	Meander 18 × 5 mm ²	20 × 50	8.8	-15.3	-21.7

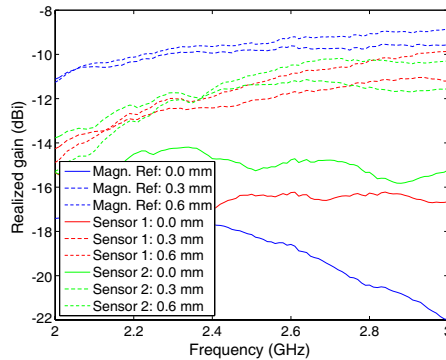


Figure 10. Measured maximum realized gain in dBi as a function of distance to the body.

at 2.4 GHz. The ground planes of the sensor antennas were slightly smaller than that of the reference antenna, and the space required by the electronics also shifted the antenna resonance to a higher frequency. Despite this, the achieved -12 dBi gain at 2.4 GHz is sufficient for short-range communications. The total efficiency (not shown) was -17 dB for the reference antenna and -18 dB for the sensor antennas.

The measured radiation patterns in the xy and xz planes for the sensors 1 and 2 are shown in Figs. 11 and 12, respectively. The axis

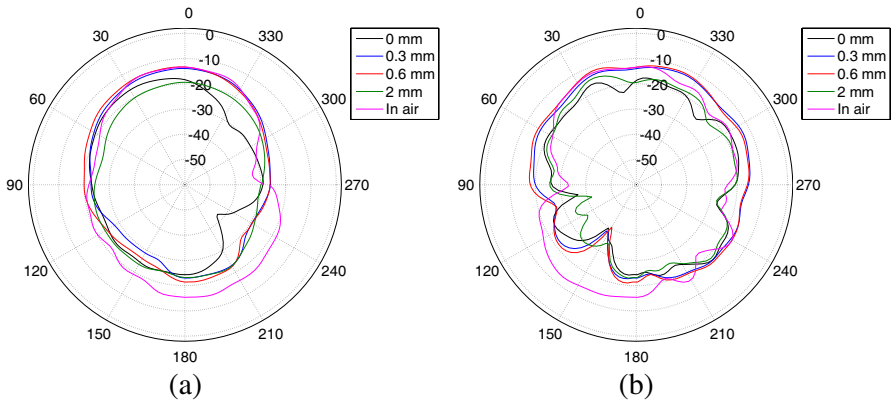


Figure 11. Measured absolute gain for sensor layout 1 (a) in xz plane and (b) in yz plane.

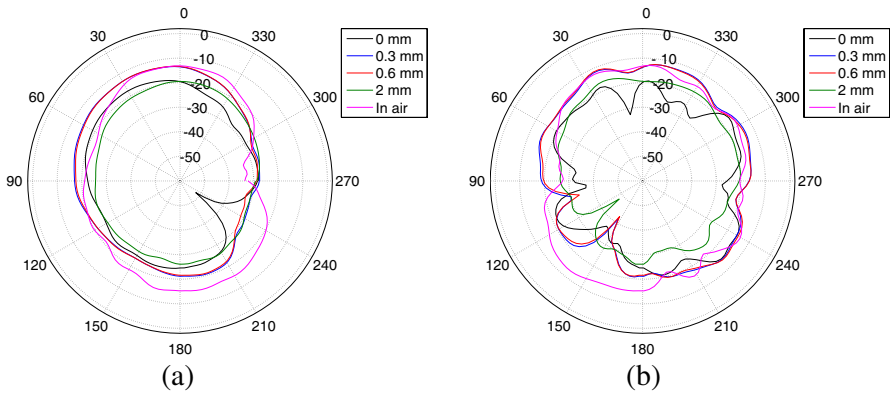


Figure 12. Measured absolute gain for sensor layout 2 (a) in xz plane and (b) in yz plane.

are defined in Fig. 9. The figures show total absolute gain in dBi, mainly due to the E_ϕ component. The main direction of radiation is approximately normal to the body, i.e., in the $\theta = 0$ direction. The antennas show similar performance at 0.3 mm and 0.6 mm from the body as in free space. This is because antennas were designed for on-body operation and the matching is not optimal in free space. The lower gain at 2 mm from the body is also due to matching whereas in direct contact the main reason is loss due to the body tissue. The difference in routing in sensors 1 and 2 does not significantly affect the radiation characteristics.

3.3. Radio Interface Test

The radio interface consisting of a system-on-chip (SoC), a filter balun circuit, and the antenna was assembled and tested. A sensor prototype is shown in Fig. 13. A solid-state battery is located on the left whereas space for sensing elements and related electronics is reserved on the right. Despite the better performance obtained with the discrete LC balun circuit, a commercial monolithic balun component was selected due to its smaller size. The radio link was tested by transmitting continuous signal at a BLE channel and measuring the received power level using a manufacturer's test board. The sensitivity of the receiver was -82 dBm.

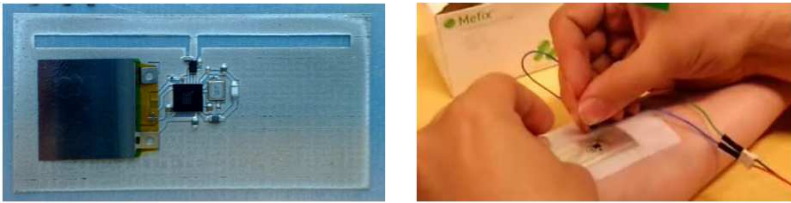


Figure 13. Inkjet-printed sensor prototype (sensor 1) and test setup for on-body operation with an external power source (sensor 2).

The test was carried out with the sensor in free space and attached on body (hand) with a 0.3-mm layer of plaster between the sensor and the body as shown in Fig. 13. An external power source was used during the test. Three different power levels were considered including $+4$ dBm, -4 dBm, and -8 dBm. For all transmission powers tested, the received power remained above -80 dBm at one meter from the body. This is sufficient for short-range off-body communications demonstrating the potential of inkjet-printed single-layer sensors for biomedical applications.

4. CONCLUSION

This work demonstrates the design and implementation of thin, lightweight and flexible single-layer inkjet-printed wireless sensors for biomedical applications. Discrete RF electronics and single-layer antennas operating at 2.4 GHz were successfully designed and verified by measurements. At 0.3 mm from the body, 2.4 dB insertion loss and -10 dBi realized gain were achieved for the discrete filter balun and antenna, respectively. Finally, the radio interface of a fully functional wireless sensor was implemented and tested. Regardless

of a commercial monolithic filter balun with 4 dB insertion loss and a slightly off-tuned sensor antenna with -12 dBi gain at 2.4 GHz, the sensor placed at 0.3 mm from the body achieved one meter transmission distance. This is sufficient for short-range off-body communications in biomedical sensor applications.

ACKNOWLEDGMENT

This work is funded by the Academy of Finland and The Finnish Funding Agency for Technology and Innovation.

REFERENCES

1. Vuorela, T., J. Hännikäinen, and J. Vanhala, "Plaster like physiological signal recorder design process, lessons learned," *Proc. Ambience 08 Smart Textiles — Technology and Design*, 89–96, Boras, Sweden, Jun. 2008.
2. Singh, M., H. Haverinen, P. Dhagat, and G. Jabbour, "Inkjet printing process and its applications," *Advanced Materials*, Vol. 22, No. 6, 673–685, 2010.
3. Mäntysalo, M., V. Pekkanen, K. Kaija, J. Niittynen, S. Koskinen, E. Halonen, P. Mansikkamäki, and O. Hämeenoja, "Capability of inkjet technology in electronics manufacturing," *Proc. 59th Electronic Components and Technology Conf.*, 1330–1336, San Diego, CA, May 2009.
4. Mäkinen, R., H. Sillanpää, and J. Jalo, "State-of-the-art in characterization-based printed electronics RF design," *Proc. IEEE Wireless and Microwave Technol. Conf.*, 4, Apr. 2013.
5. Orecchini, G., F. Alimenti, V. Palazzari, A. Rida, M. Tentzeris, and L. Roselli, "Design and fabrication of ultra-low cost radio frequency identification antennas and tags exploiting paper substrates and inkjet printing technology," *IET Microw. Antennas Propag.*, Vol. 5, No. 8, 993–1001, 2011.
6. Pynttäre, V., E. Halonen, H. Sillanpää, M. Mäntysalo, and R. Mäkinen, "RF design for inkjet technology: Antenna geometries and layer thickness optimization," *IEEE Antennas Wireless Propagation Lett.*, Vol. 11, 188–191, 2012.
7. Hall, P. S. and Y. Hao, *Antennas and Propagation for Body-centric Wireless Communications*, 2nd Edition, Artech House, London, 2012.
8. Alomainy, A., Y. Hao, and D. Davenport, "Parametric study of wearable antennas with varying distance from the body and

- different on-body positions,” *Proc. IET Antennas Propagat. for Body-centric Wireless Commun.*, 84–89, London, UK, 2007.
9. Kellomäki, T., “Effects of the human body on single-layer wearable antennas,” Ph.D. Thesis, Tampere University of Technology, Tampere, 2012.
 10. Kellomäki, T. and R. Mäkinen, “Magnetic and electric antennas close to the body,” *Proc. IEEE Antennas Propagat. Intl. Symp.*, 2, Jul. 2013.
 11. Kellomäki, T., “On-body performance of a wearable single-layer RFID tag,” *IEEE Antennas and Wireless Propagation Lett.*, Vol. 12, 73–76, 2012.
 12. Jais, M. I., M. F. B. Jamlos, M. Jusoh, T. Sabapathy, M. R. Kamarudin, R. B. Ahmad, A. A. A.-H. Azremi, E. I. Bin Azmi, P. J. Soh, G. A. E. Vandenbosch, and N. L. K. Ishak, “A novel 2.45 GHz switchable beam textile antenna (SBTA) for outdoor wireless body area network (WBAN) applications,” *Progress In Electromagnetics Research*, Vol. 138, 613–627, 2013.
 13. Paul, D. L., H. Giddens, M. G. Paterson, G. S. Hilton, and J. P. McGeehan, “Impact of body and clothing on a wearable textile dual band antenna at digital television and wireless communications bands,” *IEEE Transactions on Antennas and Wireless Propagation*, Vol. 61, No. 4, 2188–2194, Apr. 2013.
 14. Akhoondzadeh-Asl, L., Y. Nechayev, P. S. Hall, and C .C. Constantinou, “Parasitic array antenna with enhanced surface wave launching for on-body communications,” *IEEE Transactions on Antennas and Wireless Propagation*, Vol. 61, No. 4, 1976–1985, Apr. 2013.
 15. Alam, S., H. P. Sillanpää, and R. M. Mäkinen, “Human body effects on inkjet-printed flexible RF interconnections,” *Progress In Electromagnetics Research C*, Vol. 35, 83–94, 2013.
 16. Sillanpää, H., S. Alam, and R. Mäkinen, “Printed electronics design for body-worn wireless applications,” *Proc. IEEE Wireless and Microwave Technol. Conf.*, 4, Apr. 2013.
 17. Enderling, S., et al., “Sheet resistance measurement of non-standard cleanroom materials using suspended Greek cross test structures,” *IEEE Trans. Semicond. Manuf.*, Vol. 19, No. 1, 2–9, 2006.
 18. Sillanpää, H., A. Rasku, and R. Mäkinen, “A multiline material parameter extraction method,” *Proc. 10th Mediterranean Microwave Symp.*, 314–317, Guzelyurt, Cyprus, 2010.

19. Rasku, A., H. Sillanpää, I. Hiltunen, and R. Mäkinen, “Multiline material parameter extraction method performance analysis,” *Proc. Asia-Pacific Microwave Conf.*, 1905–1908, Yokohama, Japan, Dec. 2010.
20. Sillanpää, H., A. Rasku, and R. Mäkinen, “Application of a multiline material characterization method to inkjet printed electronics,” *International Journal of RF and Microwave Computer-aided Engineering*, 7, 2013, DOI: 10.1002/mmce.20746.
21. Marks, R. B., “A multiline method of network analyzer calibration,” *IEEE Trans. Microwave Theory Tech.*, Vol. 39, No. 7, 1205–1215, 1991.
22. Gabriel, C., “Compilation of the dielectric properties of body tissues at RF and microwave frequencies,” Tech. Rep. AL/OE-TR-1996-0037, Brooks Air Force, 1996.
23. Lee, S., “Using single-ended S -matrices to characterize differential components in mobile radio design,” *RF Design*, 14–18, 2003.
24. Bockelman, D. E. and W. R. Eisenstadt, “Combined differential and common-mode scattering parameters: Theory and simulation,” *IEEE Trans. Microwave Theory Tech.*, Vol. 43, No. 7, 2–9, 1995.